ARTICLE

OBC
www.rsc.org/obc

Specificity in template syntheses of hexaaza-macrobicyclic cages: $[Pt(Me_5\text{-tricosatrieneN}_6)]^{4+}$ and $[Pt(Me_5\text{-tricosaneN}_6)]^{4+}$ †

Kylie N. Brown,[a] Rodney J. Geue,[a] Trevor W. Hambley,[b] David C. R. Hockless,[a] A. David Rae[a] and Alan M. Sargeson*[a]

[a] *Research School of Chemistry, Australian National University, A.C.T., 0200, Australia*
[b] *School of Chemistry, University of Sydney, NSW, 2006, Australia*

Received 16th December 2002, Accepted 12th March 2003
First published as an Advance Article on the web 3rd April 2003

The racemic C_3 hexadentate cage complex, $[Pt(Me_5\text{-tricosatrieneN}_6)]Cl_4$ (1,5,9,13,20-pentamethyl-3,7,11,15,18,22-hexaazabicyclo[7.7.7]tricosa-3,14,18-triene)platinum(IV) tetrachloride), was synthesised stereospecifically and regiospecifically from a reaction of the bis-triamine template $[Pt(tame)_2]Cl_4$ (bis[1,1,1-tris(aminomethyl)ethane]-platinum(IV) tetrachloride) with formaldehyde and then propanal, in acetonitrile under basic conditions. Largely, one racemic diastereoisomer was obtained in a surprisingly high yield (~ 50%), even though the molecule has seven chiral centres. The origins of the stereoselective synthesis are addressed. The crystal structure of $[Pt(Me_5\text{-tricosatrieneN}_6)](ZnCl_4)_{1.5}Cl\cdot 2H_2O$ showed that all three imines were attached to one tame fragment with a chiral amine site (ΛSSS, ΔRRR) and a chiral methine carbon site (ΛRRR, ΔSSS) on each ligand strand. The PtN_6^{4+} moiety had a slightly distorted octahedral configuration with the two types of Pt–N bonds related to the imine and the amine donors, 2.050(7) and 2.072(6) Å, respectively. Treatment with sodium borohydride (15 s, 20 °C) at pH ~ 12.5 reduced the imine groups, but not the Pt(IV) ion, producing a C_3 saturated ligand complex $[Pt(Me_5\text{-tricosaneN}_6)]Cl_4$ ((1,5,9,13,20-pentamethyl-3,7,11,15,18,22-hexaazabicyclo[7.7.7]tricosane)platinum(IV)tetrachloride). X-ray crystallographic analysis showed that the average Pt–N bond distance in the cation increased upon imine reduction to 2.10 (av) Å. The cyclic voltammograms of the two cage complexes displayed irreversible two-electron reduction waves in aqueous media and a ~ 0.3 V shift to more positive potentials compared to that of the smaller cavity sar (3,6,10,13,16,19-hexaazabicyclo[6.6.6]icosane) analogue. After reduction, net dissociation of one strand of the cage was also evident, to give unstable square planar Pt(II) macrocyclic products.

Introduction

This paper explores the use of the achiral octahedral template $[Pt(tame)_2]^{4+}$ (bis[1,1,1-tris(aminomethyl)ethane-*N*,*N*′,*N*″]-platinum(IV), **1**) for synthesising organic cages about the metal ion following successful stereoselective syntheses of such sophisticated complexes using Co(III) analogues.[1–3]

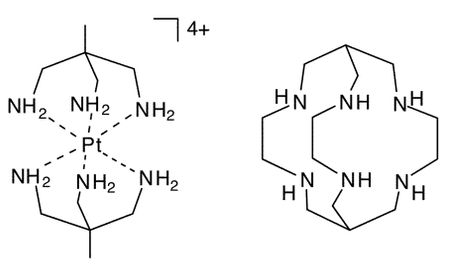

1

2

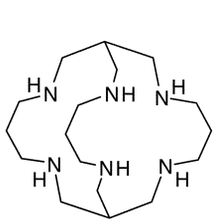

3

An important prospect of encapsulating metal ions with the cage ligands sar‡ (**2**) and tricosaneN_6 (**3**) is that reactive oxidation states may be stabilised since the encapsulating nature and steric constraints of such ligands tend to enforce 6-coordination and hinder dissociation, substitution and dimerisation reactions. Examples include the stabilisation of the reactive d^7 states, such as Co(II)[3–5] and Rh(II)[6,7]. It had been anticipated that Pt(III) sar complexes might be stabilised following reduction of analogous Pt(IV) complexes[8–10] but this strategy had only limited success. One of the unexpected features was their different electrochemical behaviour in acetone and in water.[8,9] For example, the $[Pt^{III}((NHOH)_2sar)]^{3+}$ transient was observed by EPR techniques and by γ- and pulse radiolysis in water at 25 °C. However, on a longer timescale, electrochemical studies of the Pt(IV)sar complex (in acetone at 193 K) implied that the processes in Scheme 1 took place.[8,9] The Pt(IV) ion is first reduced to Pt(III), which then homolyses to form a Pt(III)–$N^{\bullet}$ radical moiety and a hydrogen atom. Two hydrogen atoms then combine to form dihydrogen on the surface of the electrode and intramolecular electron transfer forms the deprotonated Pt(IV) reactant.

This electrochemical behaviour was attributed to stress in the ligand arising from the larger Pt(III) ion. The seventh d electron in the Pt(III) system would occupy an antibonding e_g* orbital

† Electronic supplementary information (ESI) available: tables of hydrogen atom position parameters, displacement parameters and torsional angles for all crystal structures and some electrochemical data and NMR spectral data for the hydrogenation of $[Pt(Me_5\text{-tricosatrieneN}_6)]Cl_4$. See http://www.rsc.org/suppdata/ob/b2/b212326f/

‡ Abbreviated ligand names used in this paper: sar, sarcophagine: 3,6,10,13,16,19-hexaazabicyclo[6.6.6]icosane; sep, sepulchrate: 1,3,6,8,10,13,16,19-octaazabicyclo[6.6.6]icosane; Me_5-tricosaneN_6: 1,5,9,13,20-pentamethyl-3,7,11,15,18,22-hexaazabicyclo[7.7.7]tricosane; Me_5-tricosanetriimineN_6: 1,5,9,13,20-pentamethyl-3,7,11,15,18,22-hexaazabicyclo[7.7.7]tricosa-3,18,15-triene; tame: 1,1,1-tris(aminomethyl)-ethane; [9]aneN_3: 1,4,7-triazacyclononane; Et_2-Me_6-tetracosane-diimineN_6: 19,23-diethyl-1,5,9,13,20,24-hexamethyl-3,7,11,15,18,22-hexaazatricyclo[10.4.4.4$^{4-9}$]tetracosa-3,11-diene.

DOI: 10.1039/b212326f

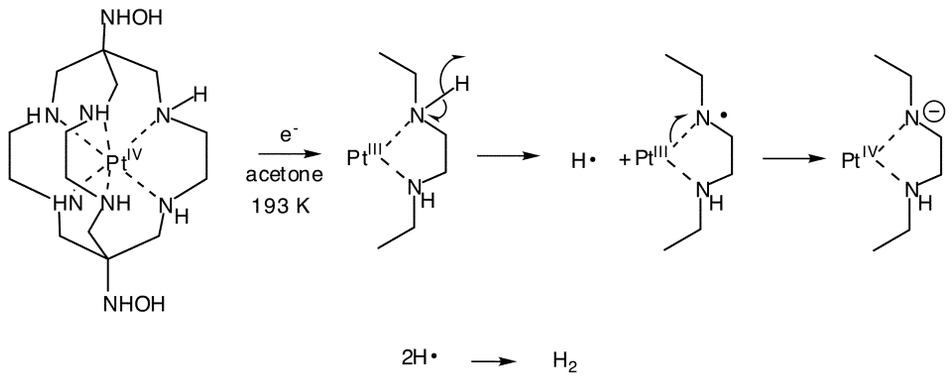

Scheme 1 Reduction of $[Pt((NHOH)_2sar)]^{4+}$, in acetone at 193 K.

co-aligned with one of the Pt–N axes. The increased electron density and consequent increased Pt–N bond length presumably influences the adjacent N–H bond, leading to its homolytic fission and relief of the stress in the formation of the deprotonated Pt^{IV}–N^- complex. Reprotonation would then regenerate the reactant and turnover would allow it to function as an effective electrocatalyst for dihydrogen production at low overpotential. In aqueous media, however, the Pt(III) intermediate in the bulk electrolysed solution led to a mixture of both Pt(II) and Pt(IV) macrocyclic complexes.[8,9] Presumably, after reduction to the Pt(III) species had occurred, the ligand framework ruptured at the N–C bond to form a N anion and a carbon radical which then disproportionated, intermolecularly, to the Pt(II) and Pt(IV) species. These events, therefore, obviated the possibility of catalytic H_2 production in water with these complexes.

It is not so obvious why ligand rupture occurs at two different sites of the ligand framework, depending on solvent, acid and temperature. However, rupture of the cage might be driven simply by strain induced by the larger d^7 Pt(III) and a ligand with a larger cavity could alleviate this problem. Like Pt(III), monomeric Rh(II) complexes are rare and usually have only been detected electrochemically or by pulse radiolysis.[11] However, it has been noted that the reduction of the Rh(III) ion to Rh(II) is more favourable in the larger cavity tricosaneN_6 cages than in the analogous sar series. For example, the reduction potential for the $[Rh(Me,NH_3\text{-tricosane}N_6)]^{4+/3+}$ couple is 0.4 V more positive than that of the homologous $[Rh(Me,NH_3\text{-sar}]^{4+/3+}$ couple,[7] implying that the tricosaneN_6 ligand stabilises the Rh(II) ion more effectively than does the sar ligand. It was hoped, therefore, that the electrochemical behaviour of the analogous $[Pt(\text{tricosane}N_6)]^{4+}$ system would be similar and that a homogeneous reagent for the generation of dihydrogen at a low overvoltage would result and the cage would remain intact. This paper addresses the synthesis of such larger cage systems and their properties.

Results

Synthesis

The condensation reaction of $[Pt(tame)_2]Cl_4$ (or its triflate salt) with aqueous formaldehyde, propanal, triethylamine and anhydrous sodium perchlorate in acetonitrile gave the C_3 racemic $[Pt(Me_5\text{-tricosatriene}N_6)]Cl_4$ complex in a surprisingly high yield (~ 50%). After cation exchange chromatography of the reaction mixture, the complex was isolated as a white powder. A ^1H NMR spectrum of the mother liquor indicated that various other complexes had also formed in low yield. This mixture may contain some of the other possible cage isomers, for example, those arising from different chiralities about the secondary nitrogen and methine carbon atoms as well as non-cage complexes where two chelate rings have been formed *trans* to each other across the template. Clearly, however, one product dominates the synthetic pathway.

The $[Pt(Me_5\text{-tricosatriene}N_6)]^{4+}$ ion is unusually acidic and readily deprotonates in water to give an orange solution. However, it is stable indefinitely in aqueous solutions at pH ≤ 6. Selective reduction of the imines rather than the metal ion was unproductive using various reductants under conditions that had been successful for imine complexes of Co(III)[2,3,12–15] and Cr(III).[2] However, treatment of the complex with sodium borohydride at pH > 12.5 for not more than 15 seconds quantitatively yielded the desired saturated Pt(IV) complex. The reaction at high pH ensures that borohydride ion acts as a hydride donor selectively to the imines. At lower pH, BH_3 or B_2H_6 is formed which reacts readily with the metal centre to produce Pt(II) and Pt(0) species.

Crystal structures

An X-ray crystallographic analysis established the structure of the cation in $[Pt(Me_5\text{-tricosatriene}N_6)](ZnCl_4)_{1.5}Cl_2H_2O$ as a C_3 molecular ion (Fig. 1). The interatomic distances and angles are listed in Table 1. Other relevant crystallographic data are in Table 2. The crystal structure is necessarily disordered. The reference $[Pt(Me_5\text{-tricosatriene}N_6)]^{4+}$ cation lies at approximately 0, 0, 3/8 on a three-fold rotation axis in the space group $R\bar{3}c$. The structure is described in terms of sections $c/12$ wide. The reference cation lies midway between the plane $z = 1/3$ containing centres of inversion at 1/6, 1/3, 1/3 *etc.*, and the plane $z = 5/12$ containing two-fold rotation axes perpendicular to **c**, *i.e.* $2/3-x$, $1/3-x+y$, $5/6-z$ *etc*. The contents of such a section comprising three of the 36 asymmetric units of $R\bar{3}c$ are shown in Fig. 2.

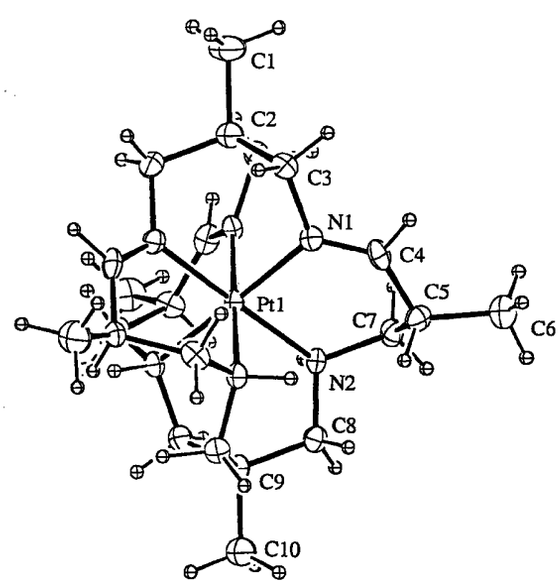

Fig. 1 ORTEP diagram of the cation in $[Pt(Me_5\text{-tricosatriene}N_6)](ZnCl_4)_{1.5}Cl{\cdot}2H_2O$.

Table 1 Interatomic distances (Å) and selected bond angles (°) for $[Pt(Me_5\text{-tricosatrieneN}_6)](ZnCl_4)_{1.5}Cl{\cdot}2H_2O$

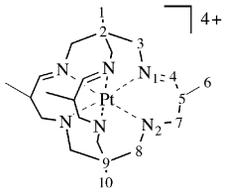

Bond distance/Å		Bond distance/Å	
Pt–N(1)	2.050(7)	Pt–N(2)	2.072(6)
C(2)–C(1)	1.575(27)	C(3)–N(1)	1.497(11)
C(3)–C(2)	1.527(27)	C(4)–N(1)	1.277(10)
C(5)–C(4)	1.470(42)	C(6)–C(5)	1.503(13)
C(7)–N(2)	1.475(11)	C(7)–C(5)	1.538(13)
C(8)–N(2)	1.508(11)	C(9)–C(8)	1.517(11)
C(10)–C(9)	1.533(27)		

Bond angles/°		Bond angles/°	
N(1)–Pt(1)–N(2)	92.1(3)	N(1)–Pt(1)–N(1)[a]	87.2(3)
N(1)–Pt(1)–N(2)[b]	91.7(3)	N(2)–Pt(1)–N(2)[a]	89.0(3)
N(1)–Pt(1)–N(2)[a]	178.7(2)		
Pt(1)–N(1)–C(3)	115.3(6)	Pt(1)–N(1)–C(4)	125.5(6)
Pt(1)–N(2)–C(7)	116.0(5)	Pt(1)–N(2)–C(8)	113.7(5)
C(3)–N(1)–C(4)	119.0(7)	C(7)–N(2)–C(8)	113.4(6)
N(1)–C(3)–C(2)	109.9(10)	N(2)–C(8)–C(9)	114.0(9)
N(1)–C(4)–C(5)	126.4(8)	N(2)–C(7)–C(5)	114.4(5)
C(1)–C(2)–C(3)	107.6(8)	C(8)–C(9)–C(10)	108.2(8)
C(4)–C(5)–C(6)	113.9(8)	C(4)–C(5)–C(7)	109.3(6)
C(6)–C(5)–C(7)	108.5(8)		

[a] $-y,x-y,z$. [b] $-x+y,-x,z$. [c] $\frac{1}{3}-x,\frac{2}{3}-y,\frac{2}{3}-z$. [d] $-x,-x+y,½-z$. [e] $-\frac{1}{3}+x,\frac{1}{3}+x-y,-1/6+z$.

Interatomic distances in the disordered structure indicate that a hydrogen-bonded ring of three-fold rotation symmetry is formed about the axis 2/3, 1/3, z in just one of the two two-fold rotation related orientations that exist in the average structure (Fig. 2). Equivalent positions of atoms Zn(1), Cl(1) and O(2) lie approximately on the two-fold axis at x = 1/3, z = 5/12 which relates cations at ~ 0, 0, 3/8 and ~ 2/3, 1/3, 11/24 and centres of inversion at 1/6, 1/3, 1/3 and 1/2, 1/2, 1/2. Either a chloride ion

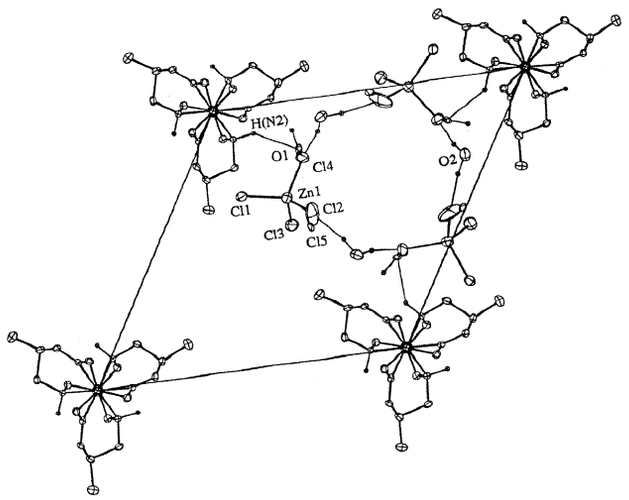

Fig. 2 Cell contents for $[Pt(Me_5\text{-tricosatrieneN}_6)](ZnCl_4)_{1.5}Cl{\cdot}2H_2O$.

or a water molecule is associated with such inversion centres of the average structure. To obtain the correct charge balance, the occupancy ratio of Cl(5) : O(1) must be 2 : 1. The Cl(5) and O(1) atoms do not lie exactly on the inversion centres of the average structure and at 1/6, 1/3, 1/3 say, only one atom exists per inversion centre. In Fig. 2, O(1) at ~ 1/6, 1/3, 1/3 is shown to be hydrogen-bonded to Cl(4), and Cl(5) at ~ 1/2, 1/2, 1/2 is shown to be in close contact with Cl(2). Atoms Cl(4) are at shorter distances from the centres of inversion than are atoms Cl(2) and only O(1) can fit between Cl(4) and its nearest centre of inversion. Whereas, either Cl(5) or O(1) can fit between Cl(2) and its nearest centre of inversion. The centre of inversion at 1/6, 1/3, 1/3 relates the 32 symmetry sites at 1/3, 2/3, 5/12 and 0, 0, 1/4. Hydrogen bonding involving the proton on N(2) of the reference asymmetric unit is directed towards the centre of inversion at 1/6, 1/3, 1/3 and the reference equivalent positions for Cl(5) and O(1) are those that form the shortest hydrogen bonds.

The configuration about the Pt(IV) ion is slightly distorted from an octahedron; the two tame residues are connected by three six-membered chelate rings at the amines (referred to as "straps"). Each of these straps bears an imine, and all three imines are connected to the same tame residue on one face of

Table 2 Crystal data

	$[Pt(Me_5\text{-tricosatrieneN}_6)](ZnCl_4)_{1.5}Cl{\cdot}2H_2O$	$[Pt(Me_5\text{-tricosaneN}_6\text{–}0.123H)](H_2OZnCl_3)_{2.123}(ZnCl_4)_{0.877}{\cdot}H_2O$
Empirical formula lattice parameters	$C_{22}H_{46}Cl_7N_6O_2PtZn_{1.5}$	$C_{22}H_{54.123}Cl_{9.877}N_6O_{3.123}PtZn_3$
a/Å	14.724 (5)	23.502 (9)
b/Å	14.724 (5)	15.453 (3)
c/Å	55.80 (1)	13.680 (4)
	γ = 120°	β = 118.66 (2)°
V/Å^3	10476 (6)	4360 (2)
Z	12	4
fw	967.98	1194.20
D_{calc}/g cm^{-3}	1.841	1.819
Space group	$R\bar{3}c$	Cc (#9)
Crystal system	Hexagonal	Monoclinic
Temp./°C	21	23
Radiation	Mo K_α (λ = 0.7107 Å), graphite monochromated	Mo K_α (λ = 0.7107 Å), graphite monochromated
μ/cm^{-1}	60.61	54.54
Scan type	ω–0.67θ	ω–2θ
Scan range/deg in 2θ	$1 < \theta < 25$	6.0–50.1
No. reflections		
total	6497	4111
unique	2066	4007
No. of data used in refinement	1480 [$I > 3\sigma(I)$]	3276 [$I > 3\sigma(I)$]
Residuals: R; R_w	0.046; 0.088	0.027; 0.036
Function minimised	$R = \Sigma w(\|F_o\| - \|F_c\|)^2$	$R = \Sigma w(\|F_o\| - \|F_c\|)^2$
Least squares weights	$1.0/\{\sigma^2(F) + (0.0016)F^2\}$	$1.0/\{\sigma^2(F) + (0.00022)F^2\}$
Decay	8.1% decline	1.7% decline

the octahedron, to form a *facial*-triimine complex. The imines force the three annular six-membered chelate rings to adopt a flattened skew-boat conformation with the methyl groups equatorially disposed. There are seven chiral centres in the complex, three arising from the secondary nitrogen atoms, three from the methine carbon atoms in the strap and one from the Pt(IV) ion. Although theoretically, there are 24 diastereoisomeric racemates of the *facial* triimine complex, ~ 50% of the total reaction mixture is composed of the Λ-isomer, shown in Fig. 1, and its mirror image. The Λ-configuration supports *S*-configurations at all three secondary nitrogen atoms and *R*-configurations about the methine carbon atoms of the straps. The crystal structure is also representative of the total isolated product.

Total reduction of the imines in the $[Pt(Me_5\text{-tricosatriene-}N_6)]^{4+}$ ion was established by NMR spectroscopy and an X-ray crystallographic analysis of a single crystal of the product containing 88% of the $[Pt(Me_5\text{-tricosaneN}_6)]^{4+}$ cation and 12% of the mono-deprotonated form (see the Experimental section for a detailed analysis of the refinement, 2.7%). Only the 4+ cation was well defined and it is depicted as an ORTEP plot in Fig. 3. Interatomic distances and angles, and other relevant crystallographic data are listed in Tables 2 and 3.

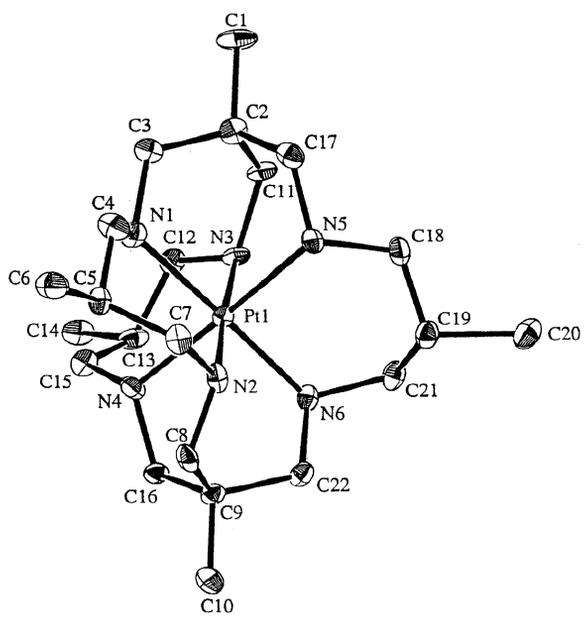

Fig. 3 ORTEP diagram of the 4+ cation in $[Pt(Me_5\text{-tricosaneN}_6\text{–}0.123H)](H_2OZnCl_3)_{2.123}(ZnCl_4)_{0.877}\cdot H_2O$.

The PtN_6 moiety is slightly distorted from an octahedral configuration. The reduction of the imines resulted in an increase in the former Pt(IV)–N_{imine} bond lengths by ~ 0.05 Å, and the Pt(IV)–N_{amine} bonds by ~ 0.03 Å. The average Pt(IV)–N bond length is 2.10 Å which is marginally shorter than the longest Pt(IV)–N bond length in a related cage complex $[Pt(Et_2\text{-}Me_6\text{-tetracosadieneN}_6\text{–H})](PF_6)_3\cdot 5H_2O$.[1] All three six-membered chelate rings forming the straps adopt a somewhat flattened-chair conformation. For the Λ configuration about the Pt(IV) ion, all the nitrogen atoms support an *S*-configuration and the methyl groups on the strap methine carbon atoms are all oriented equatorially in the same sense to give an overall C_3 configuration for the cation.

NMR Spectroscopy

The NMR spectroscopy of the $[Pt(Me_5\text{-tricosatrieneN}_6)]^{4+}$ complex in neutral and acidic conditions reflects the three-fold symmetry (Fig. 4a) displayed by the X-ray structural analysis. The DQF COSY spectrum was necessary for the assignment of the signals. The nitrogen protons in both Pt(IV) complexes

Table 3 Selected interatomic distances (Å) and bond angles (°) for $[Pt(Me_5\text{-tricosaneN}_6\text{–}0.123H)](H_2OZnCl_3)_{2.123}(ZnCl_4)_{0.877}\cdot H_2O$

Bond distance/Å		Bond distance/Å	
Pt(1)–N(1)	2.113(9)	Pt(1)–N(2)	2.11(1)
Pt(1)–N(3)	2.102(9)	Pt(1)–N(4)	2.059(9)
Pt(1)–N(5)	2.159(9)	Pt(1)–N(6)	2.079(9)
N(1)–C(3)	1.52(2)	N(1)–C(4)	1.54(1)
N(2)–C(7)	1.47(1)	N(2)–C(8)	1.50(2)
N(3)–C(11)	1.50(1)	N(3)–C(12)	1.49(1)
N(4)–C(15)	1.53(1)	N(4)–C(16)	1.50(2)
N(5)–C(17)	1.51(2)	N(5)–C(18)	1.49(1)
N(6)–C(21)	1.44(1)	N(6)–C(22)	1.49(1)
C(1)–C(2)	1.59(2)	C(2)–C(3)	1.50(2)
C(2)–C(11)	1.59(2)	C(2)–C(17)	1.50(2)
C(4)–C(5)	1.48(2)	C(5)–C(6)	1.57(2)
C(5)–C(7)	1.50(2)	C(8)–C(9)	1.48(2)
C(9)–C(10)	1.49(3)	C(9)–C(16)	1.56(2)
C(9)–C(22)	1.51(2)	C(12)–C(13)	1.51(2)
C(13)–C(14)	1.52(2)	C(13)–C(15)	1.50(2)
C(18)–C(19)	1.47(2)	C(19)–C(20)	1.59(2)
C(19)–C(21)	1.52(2)		
Angle/°		**Angle/°**	
N(1)–Pt(1)–N(2)	95.0(4)	N(1)–Pt(1)–N(3)	88.4(4)
N(1)–Pt(1)–N(4)	89.7(4)	N(1)–Pt(1)–N(5)	87.9(4)
N(1)–Pt(1)–N(6)	176.4(4)	N(2)–Pt(1)–N(3)	175.1(5)
N(2)–Pt(1)–N(4)	88.0(4)	N(2)–Pt(1)–N(5)	88.3(4)
N(2)–Pt(1)–N(6)	88.5(4)	N(3)–Pt(1)–N(4)	95.6(4)
N(3)–Pt(1)–N(5)	88.2(4)	N(3)–Pt(1)–N(6)	88.2(4)
N(4)–Pt(1)–N(5)	175.4(5)	N(4)–Pt(1)–N(6)	89.4(4)
N(5)–Pt(1)–N(6)	93.2(4)	Pt(1)–N(1)–C(3)	115.3(7)
Pt(1)–N(1)–C(4)	117.6(7)	C(3)–N(1)–C(4)	109.4(9)
Pt(1)–N(2)–C(7)	119.7(8)	Pt(1)–N(2)–C(8)	112.0(8)
C(7)–N(2)–C(8)	108.7(9)	Pt(1)–N(3)–C(11)	114.9(7)
Pt(1)–N(3)–C(12)	118.2(7)	C(11)–N(3)–C(12)	106.7(9)
Pt(1)–N(4)–C(15)	119.3(7)	Pt(1)–N(4)–C(16)	114.0(7)
C(15)–N(4)–C(16)	110.9(9)	Pt(1)–N(5)–C(17)	113.9(7)
Pt(1)–N(5)–C(18)	119.3(8)	C(17)–N(5)–C(18)	109.0(9)
Pt(1)–N(6)–C(21)	120.1(7)	Pt(1)–N(6)–C(22)	112.7(7)
C(21)–N(6)–C(22)	110.9(9)	C(1)–C(2)–C(3)	107(1)
C(1)–C(2)–C(11)	107(1)	C(1)–C(2)–C(17)	110(1)
C(3)–C(2)–C(11)	109(1)	C(3)–C(2)–C(17)	114(1)
C(11)–C(2)–C(17)	110(1)	N(1)–C(3)–C(2)	114(1)
N(1)–C(4)–C(5)	114(1)	C(4)–C(5)–C(6)	108(1)
C(4)–C(5)–C(7)	111(1)	C(6)–C(5)–C(7)	111(1)
N(2)–C(7)–C(5)	115.0(9)	N(2)–C(8)–C(9)	112(1)
C(8)–C(9)–C(10)	106(1)	C(8)–C(9)–C(16)	111(1)
C(8)–C(9)–C(22)	115(2)	C(10)–C(9)–C(16)	109(2)
C(10)–C(9)–C(22)	107(1)	C(16)–C(9)–C(22)	108(1)
N(3)–C(11)–C(2)	115(1)	N(3)–C(12)–C(13)	117.0(9)
C(12)–C(13)–C(14)	108.8(9)	C(12)–C(13)–C(15)	111.8(9)
C(14)–C(13)–C(15)	108(1)	N(4)–C(15)–C(13)	113.6(9)
N(4)–C(16)–C(9)	110(1)	N(5)–C(17)–C(2)	116(1)
N(5)–C(18)–C(19)	113.6(9)	C(18)–C(19)–C(20)	108(1)
C(18)–C(19)–C(21)	110.4(9)	C(20)–C(19)–C(21)	109(1)
N(6)–C(21)–C(19)	114.8(9)	N(6)–C(22)–C(9)	115(1)

rapidly exchange with D_2O and were not observed (estimated $pK_a < 2$). Also, only ten sets of the anticipated eleven sets of proton signals associated with the ligand carbon atoms were observed in the ^1H NMR spectrum. Equivalent protons in each ligand strand are related by the C_3 symmetry but the protons of each methylene group are magnetically inequivalent and give rise to sets of doublets. Satellites were observed in the signals at 2.16, 2.21, 3.84 and 8.86 ppm, arising from ^{195}Pt coupling with only one in each pair of methylene protons (H_{7a}, H_{8a}, H_{3a}) and the imine (H_4) ($^3J_{Pt–H7a}$ = 57.5; $^3J_{Pt–H8a}$ = 54.4; $^3J_{Pt–H3a}$ = 42; $^3J_{Pt–H4}$ = 69.2 Hz). The DQF COSY spectrum implied that long-range coupling occurred between the imine proton (H_4) and with both cap and the strap methylene protons (respectively, H_{3a}, H_{3b} and H_{7a}). § This coupling was not observed after reduc-

§ Coupling constants obtained from DQF COSY spectra tend to be less accurate,[16] hence these smaller values are approximate: $^4J_{H3a–H4}$ = 2.8; $^4J_{H3b–H4}$ = 4.9 and $^4J_{H4–H7a}$ = 4.4 Hz.

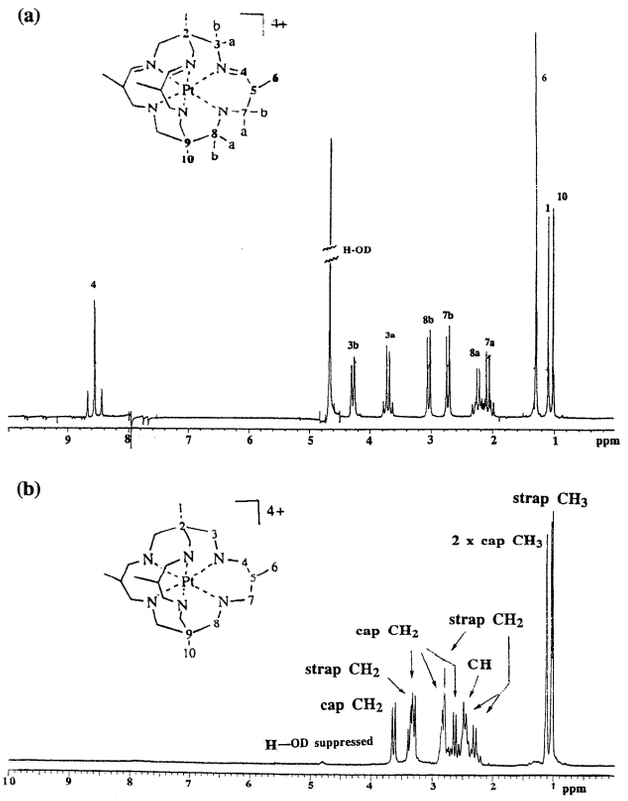

Fig. 4 ^{1}H NMR spectra of (a) [Pt(Me$_5$-tricosatrieneN$_6$)]Cl$_4$ (500 MHz) and (b) [Pt(Me$_5$-tricosaneN$_6$)]Cl$_4$ (300 MHz) in 1 M DCl, 293 K.

tion of the imines, implying that the spin–spin interaction was enhanced by the imine π-system. These protons are part of a "W" conformation, which in conjunction with the imine π-system, makes the pathway more efficient for long-range coupling.[17] The protons H_6, H_{7a} and H_{7b} exhibited relatively simple splitting patterns in the ^{1}H NMR spectrum, indicating that the methine proton (H_5) adjacent to the imine exchanges with D_2O readily, which accounts for the missing signal.

The coupling of the methine carbon atom (C_5 at δ = 35.0 ppm) with deuterium was also evident from the APT spectrum. The ^{13}C NMR spectrum of this complex is shown in Fig. 5a and also reflects the C_3 symmetry of the complex. When the methine carbon atom bears a proton, as observed in the APT spectrum of the complex in 90% H_2O–10% D_2O, its resonance is considerably sharper and has the same phase as the methyl and the imine carbon atoms. However, the HMBC spectrum was necessary to completely assign the carbon signals. Coupling of the carbon atoms with the ^{195}Pt nucleus in [Pt(Me$_5$-tricosatrieneN$_6$)]Cl$_4$ was observed for both of the quaternary carbon atoms of the caps (C_2 and C_9), the strap methine carbon atom (C_5) and to a small degree with the imine (C_4). The largest ^{195}Pt–C coupling was with the quaternary carbon atom in the tame residue connected to the saturated side of the complex, $^{3}J_{Pt-C9}$ = 54.8 Hz.

The splitting pattern in the ^{1}H NMR spectrum of the fully protonated saturated hexaamine cage complex [Pt(Me$_5$-tricosaneN$_6$)]Cl$_4$ in DCl–D_2O, Fig. 4b is similar to that observed for the analogous Co(III) complex.[3] The amine protons exchange rapidly with D_2O and are not observed as with the parent triimine (pK_a < 2). The C_3 symmetry of the cation is evident in both the ^{1}H and ^{13}C NMR spectra, Figs. 4b and 5b. The platinum coupling with one of the quaternary carbon atoms in the cap is the largest reported for a saturated PtN_6^{4+} complex ($^{3}J_{Pt-C}$ = 86 Hz) and double that in the opposite tame residue ($^{3}J_{Pt-C}$ = 41 Hz). The coupling constant in the latter instance is typical for saturated Pt(IV) hexaamine complexes.[18]

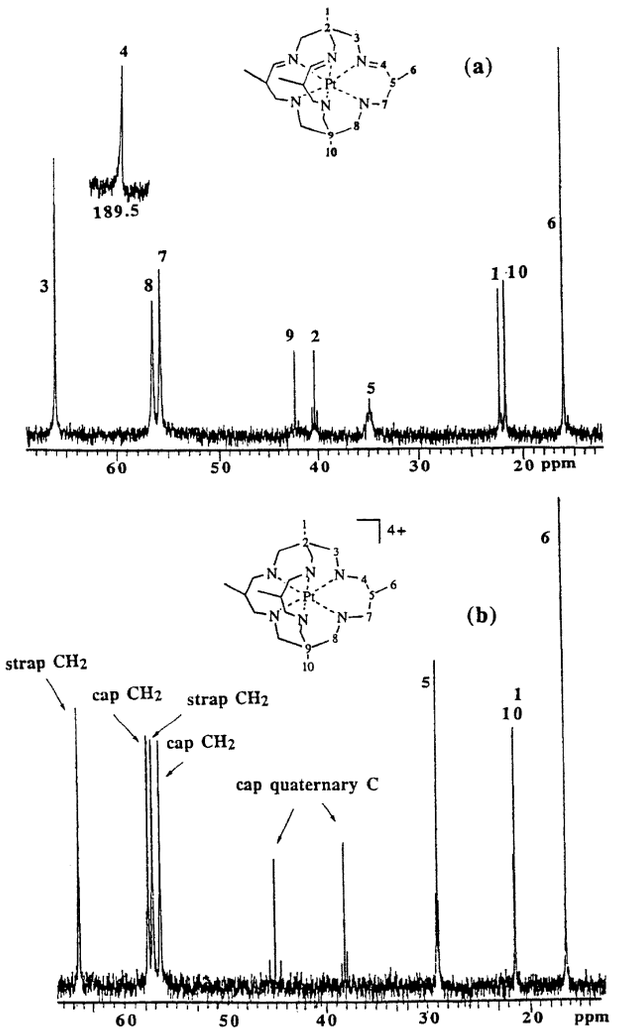

Fig. 5 300 MHz ^{13}C NMR spectra of (a) [Pt(Me$_5$-tricosatrieneN$_6$)]Cl$_4$ and (b) [Pt(Me$_5$-tricosaneN$_6$)]Cl$_4$ in 1 M DCl, 293 K.

It was thought initially that catalytic hydrogenation was a likely route for the selective reduction of the imines. However, treating [Pt(Me$_5$-tricosatrieneN$_6$)]Cl$_4$ with H_2 and 10% Pd/C catalyst at 275 K and atmospheric pressure in D_2O (initially an orange solution) gave a transient green and then a colourless solution characteristic of a Pt(II) complex. Although the reaction appeared to be complete after three hours, ^{1}H NMR signals in the imine region were still evident. The process was therefore investigated by ^{1}H and ^{13}C NMR spectrometry after 30 minutes and two hours. The ^{13}C NMR spectrum after 30 minutes of hydrogenation displayed 16 new resonances (Fig. 6a), notably, five new signals in the methyl region at 14.0, 14.6, 14.7, 17.8, 23.1 ppm, and two resonances at 94.7 and 182.3 ppm. That at 94.7 ppm is attributed to carbinolamines arising from hydration of the two imine sites in the Pt(II) macrocycle formed on reduction. The signal at 182.3 is attributed to the carbon atom of a dissociated imine. After 2 h, the reduction was almost complete (Fig. 6b) and some rearrangement of the Pt(II) macrocycle had occurred.

Similar results were displayed by the ^{1}H NMR spectra† acquired over these same periods.

A likely structure for the dominant intermediate arising from the hydrogenation is depicted as complex **B** in Scheme 5 (see ahead). The proposed complex has strictly 22 different carbon environments, but there is a pseudo mirror-plane through the detached strand which essentially bisects the Pt(II) macrocycle. This pseudo-symmetry could reduce the observable carbon signals to 16, consistent with the changes in the^{13}C NMR spectrum over 2 h hydrogenation. The many different products,

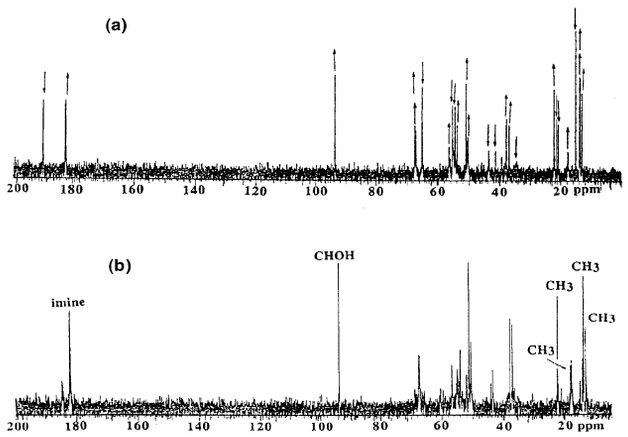

Fig. 6 300 MHz ^{13}C NMR spectra of $[Pt(Me_5\text{-tricosatrieneN}_6)]Cl_4$ taken at (a) 0.5 h, (b) 2 h of hydrogenation over a Pd/charcoal catalyst in D_2O at 293 K.

after prolonged hydrogenation, could then arise from epimerisation at carbon and nitrogen centres, rupture of the uncoordinated imine strand and possibly interchange of the bound and unbound nitrogen atoms at the Pt(II) centre.

Electrochemistry

The cyclic voltammograms (CV's) of $[Pt(Me_5\text{-tricosatrieneN}_6)]Cl_4$ in 0.1 M HCl using the EPG electrode, HMDE or gold disc electrode all showed irreversible reduction waves.[19] The electrochemical data is compiled in Table 4S (supplementary material †) and the CV's using the EPG and gold disc electrodes are shown in Fig. 7. It is proposed that the irreversible response is due to a two-electron reduction to Pt(II) (+0.2 V), by comparison with the results for the reduction of $[Pt(en)_3]^{4+}$ (−0.2 V), $[Pt(tame)_2]^{4+}$ (−0.2 V), the related cage complex $[Pt(Et_2\text{-}Me_6\text{-tetracosadieneN}_6)]^{4+}$ and the Pt(IV) sar complexes in aqueous acid conditions[2,9,20,21] (*vs.* SHE, 295 K).

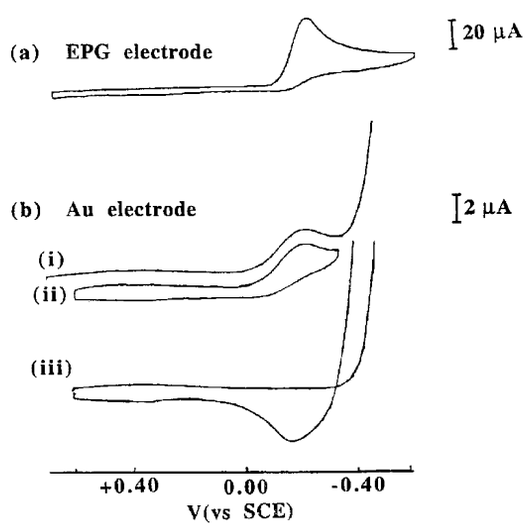

Fig. 7 Cyclic voltammograms of $[Pt(Me_5\text{-tricosatrieneN}_6)]^{4+/2+}$. (a) 0.1 M HCl, 50 mV s^{-1} (*vs.* SCE, EPG electrode); (b) 0.1 M HCl (i) and (ii) in the presence of $[Pt(Me_5\text{-tricosatrieneN}_6)]^{4+}$, (iii) in the absence of $[Pt(Me_5\text{-tricosatrieneN}_6)]^{4+}$ (50 mV s^{-1}, *vs.* SCE, Au electrode).

Similarly, all of the CV's of the saturated and fully protonated $[Pt(Me_5\text{-tricosaneN}_6)]^{4+}$ complex in aqueous 0.1 M CF_3COOH using the HMDE and gold disc electrode showed an irreversible reduction wave (+0.1 V *vs.* SHE), Pt(IV) to Pt(II) (Fig. 8 and Table 4S). The reduction potential of the saturated complex was somewhat more positive than that for the triimine

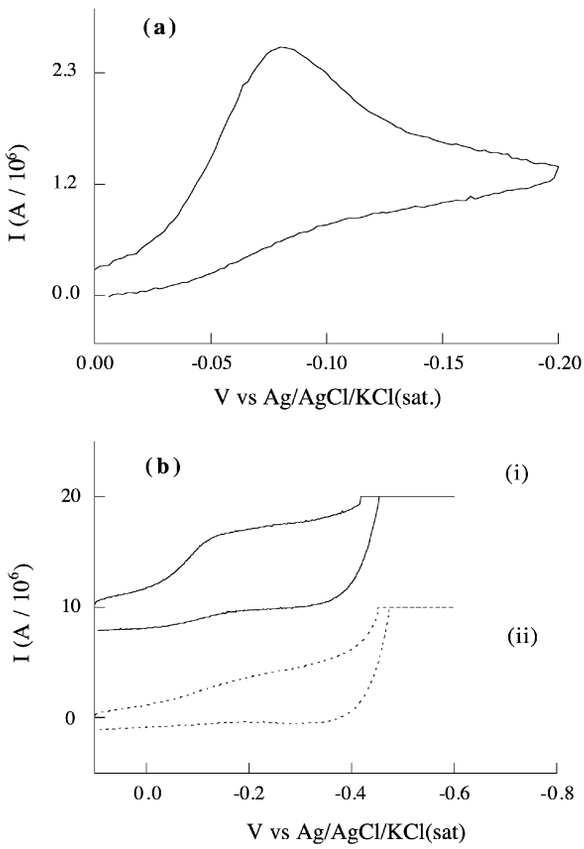

Fig. 8 Cyclic voltammograms of $[Pt(Me_5\text{-tricosaneN}_6)]^{4+/2+}$. (a) 0.1 M CF_3COOH, 100 mV s^{-1} (*vs.* Ag/AgCl/KCl(sat.), HMDE); (b) 0.1 M CF_3COOH (i) in the presence of $[Pt(Me_5\text{-tricosaneN}_6)]^{4+}$, (ii) in the absence of $[Pt(Me_5\text{-tricosaneN}_6)]^{4+}$ (100 mV s^{-1}, *vs.* Ag/AgCl/KCl(sat.), Au electrode).

under the same conditions. This pattern has also been observed for one electron reductions of analogous Co(III) systems.[3]

The potentials at which dihydrogen evolution occurred in the presence of $[Pt(Me_5\text{-tricosatrieneN}_6)]^{4+}$ (in 0.1 M HCl) and also for $[Pt(Me_5\text{-tricosaneN}_6)]^{4+}$ (in 0.1 M CF_3COOH) using the gold electrode (Figs. 7b(i) and 8b(i), respectively) are similar to that in the absence of either of these complexes (Figs. 7b(ii) and 8b(ii)). It follows that the complexes are not very effective catalysts for the electroproduction of dihydrogen at low overpotentials.

Discussion

An overview of the structures of these complexes is relevant to discussion of the synthetic pathways. The C_3 $[Pt(Me_5\text{-tricosatrieneN}_6)]^{4+}$ structure is very similar to that of the Co(III) equivalent except that the Pt(IV)–N bond lengths are longer. Both complexes have their annular six-membered chelate rings in flattened skew-boat conformations and the equatorial methyl groups are all oriented in the same sense for each isomer. Similar comments can be made for the saturated C_3 tricosaneN$_6$ complexes of both Pt(IV) and Co(III). Here, however, the annular chelate straps have distorted chair-conformations in contrast to those of the tri-imine complexes. They presumably adopt these different configurations as a result of the different overall intramolecular steric demands.

The formation and isolation of largely one cage stereoisomer and its mirror image from the reaction of $[Pt(tame)_2]Cl_4$, formaldehyde and propanal is remarkable, given that 24 isomeric pairs are theoretically possible. A mechanism accounting for this specificity is advanced in Scheme 2. A combination of inter- and intramolecular condensation reactions is involved and two stereochemical aspects are argued to dominate the degree of

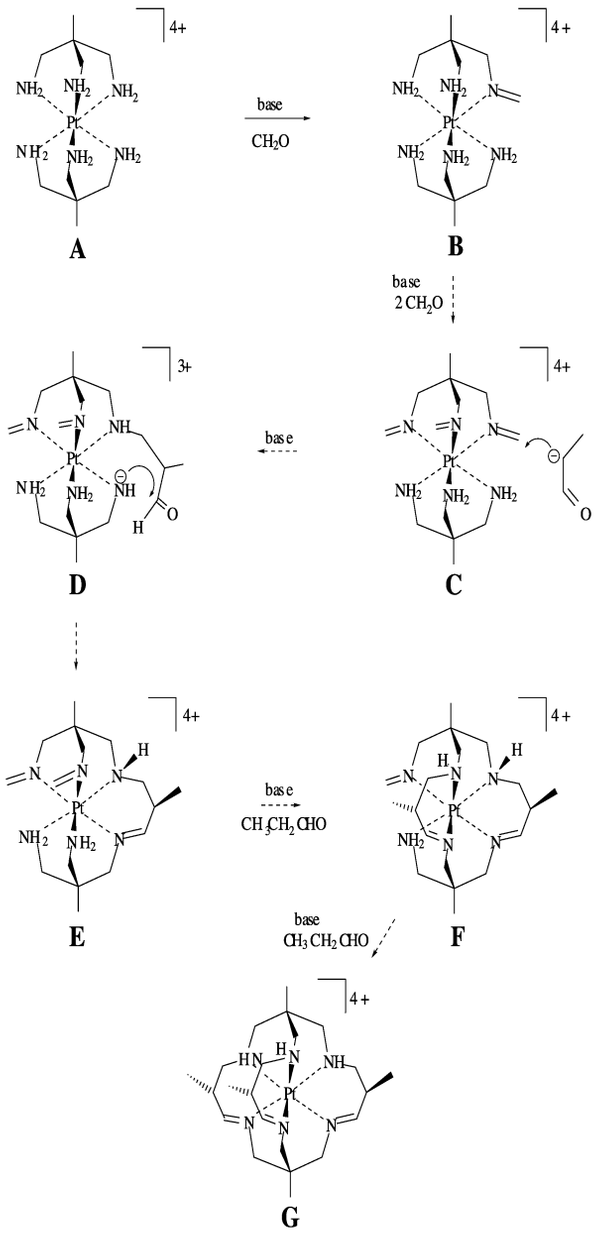

Scheme 2 Proposed mechanism for the synthesis of $[Pt(Me_5\text{-tricosatrieneN}_6)]^{4+}$.

specificity of the synthesis. Salient features are that the three imines form on one tame residue and the configurations about the methine carbon centres are the same. The latter are linked to the chirality about the Pt(IV) ion. The observed regioselectivity may result from a subtle combination of intraligand electronic and steric effects which steer the sequence of condensation reactions. The former effects are not well understood in terms of how they govern the relative acidities of coordinated amines but some insight is provided by the literature. Formation of the first imine may affect the relative acidities of the remaining uncondensed amines and the differences could be related to whether the amines are *cis* or *trans* to the coordinated imine and also on which template ligand the imine resides. Studies relating the acidities of stereoisomers of $[Pt(NH_3)_x(en)(Cl)_{x-1}(py)_y]^{n+}$ ($x = 3, 2, 1, 0$, $y = 0, 1, 2$) to electronic effects imply that amines *cis* to the pyridine groups are more acidic than those that are *trans*.[22,23] If the pyridine ligand in these systems can be regarded as an imine analogue, then amine sites *cis* to coordinated imines are likely to be more acidic than those that are *trans*. Extending this premise to the condensation reactions presented here, the remaining amines *cis* to the first imine should be more acidic. Additional support for this interpretation may be drawn from the lack of evidence for *mer* $[Pt(Me_5\text{-tricosatrieneN}_6)]^{4+}$ isomers where three imine sites lie on an octahedral meridian. Since only ~ 50% of the template was accounted for in the products, some other isomers may have formed along with various other by-products but they were not present as substantial components. Similarly, no *mer* tri-imine complexes were detected in other strapping reactions giving rise to tricosatrieneN$_6$ complexes, such as in the reaction of $[Pt(tame)_2]^{4+}$ with acetaldehyde.[2] In addition, it is feasible that this effect is more pronounced within one tame residue.

Since formaldehyde is more reactive than propanal, it is proposed that the deprotonated $[Pt(tame)_2]^{4+}$ template, **A**, condenses first with formaldehyde to form a mono-methanimine complex, **B**, (Scheme 2). Condensation of propanal with the template will only be competitive when the concentration of formaldehyde is very low, in which case other cage complexes are formed, for example $[Pt(Et_2\text{-}Me_6\text{-tetracosadieneN}_6)]^{4+}$.[1,2] Intermediate **B** condenses with a second formaldehyde, *cis* to the first imine on the same tame ligand. These two methanimines doubly activate the remaining primary amine on the same tame ligand to deprotonate and react with a third formaldehyde, to form the *facial*-tris(methanimine) complex, **C**. Intermolecular nucleophilic attack of a propanal carbanion with one of the imines produces **D**, which bears a pendant carbonyl moiety. Dreiding models indicate that the pendant carbonyl is poised for a facile intramolecular attack by an adjacent deprotonated amine on the opposite tame ligand and this condensation yields **E**, the first ligand strap. The remaining two methanimines condense sequentially with two propanal carbanions in a manner similar to that of the first imine to form **F**, the second strap and then the final complex, **G** containing all three straps.

The process in Scheme 2, however, is even more intricate since it must account for the reaction of six organic fragments with the template such that seven stereogenic centres are produced, two associated with each strap (at the secondary nitrogen and the methine carbon atoms), plus that about the Pt(IV) ion. The Λ-$[Pt(Me_5\text{-tricosatrieneN}_6)]^{4+}$ structure shows that the configurations about the three methine carbon atoms in the strap and the secondary nitrogen atoms are *R* and *S*, respectively. It is not clear whether the observed configurations are established entirely under kinetic or thermodynamic control, but clearly there is much stereochemical control overall in the process. The first strap formed decides the Δ or the Λ chirality about the metal ion and they are necessarily equally favoured. Thereafter, the condensation appears more specifically controlled as indicated in Scheme 3. The propanal carbanion

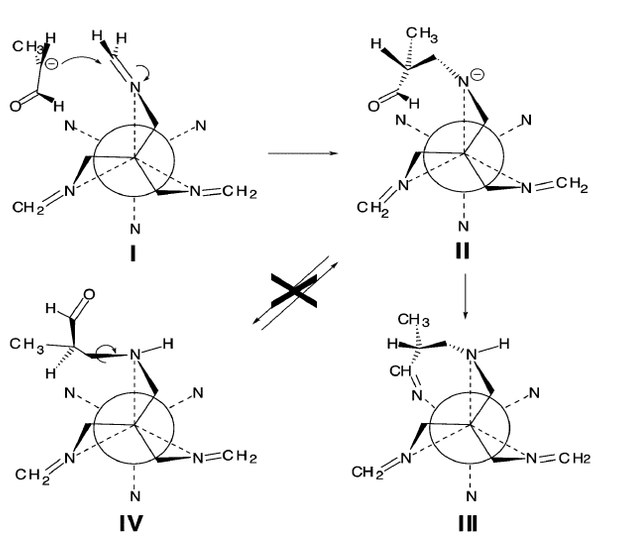

Scheme 3 Likely approach of the first propanal carbanion to the tris(methanimine) intermediate, **C**.

approaches a methanimine, oriented such that steric interactions of its carbonyl and methyl groups with the tame methylene protons and the remaining two methanimines are minimised (**I**). The methyl group is expected to be oriented away from the template and poised to adopt an equatorial position in the resultant six-membered chelate ring. Attack of the propanal carbanion at the imine creates two stereogenic centres, one at the carbanion carbon and the other at the nitrogen centre (**II**). However, the nitrogen proton rapidly exchanges with solvent so its configuration would not necessarily be controlled overall. Condensation of the pendant carbonyl with an amine on the opposite tame ligand leads to the formation of an imine at this site (**III**). If the propanal carbanion condenses at an imine with its carbonyl group oriented away from the amine on the opposite tame ligand, the intermediate **IV** results, and Dreiding models indicate that rotation about the axis shown in structure **IV** would be sterically hindered. Cyclisation is therefore inhibited by this path.

Similar steric influences pertain to the formation of the remaining straps. In forming the second strap, a propanal condenses with either of the remaining two methanimines in four possible ways, as depicted in Scheme 4. Attack by the second propanal carbanion at the face of the methanimine indicated in Scheme 4(a) is not likely. Dreiding models imply that the first strap would hinder the approach of the carbanion to this face of the imine. Hindrance is less if the propanal carbanion approaches the other side of the same imine, as depicted in Scheme 4(b). Similarly, hindrance is also less for (c) and (d). If attack takes place as in (b) or (c), then the resulting configuration about the strap methine centre will be the same as that in the first strap. However, if the carbanion approaches and condenses with the methanimine as in (d), its pendant carbonyl is more favourably aligned for condensation with the opposite tame cap, to give a complex with two straps *trans* to each other. If this occurs, formation of the third strap to form the triimine complex is obviated. However, attack at this site to give the *trans*-strapped complex is not statistically favoured by 1 : 2. Although the C_3 symmetrical isomer is favoured overall, it is evident that small amounts of other complexes of lower symmetry and incompletely condensed complexes are also formed.

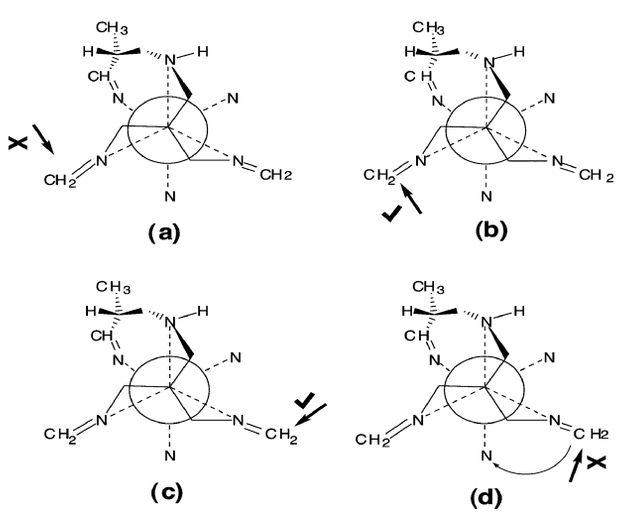

Scheme 4 Approach of the second propanal carbanion to either of the two remaining methanimines of intermediate **E**. (a) Most hindered side for attack; (b) and (c) attack from this side yields the same methine configuration as that in the first strap; (d) attack from this side yields the complex with the newly formed chelate rings *trans* to each other.

The most favoured conformation of the complex arises when the configurations about the methine centres of the six-membered chelate rings are the same, with the methyl substituents in the equatorial position. If less favoured configurations are produced in the pendant carbonyl complex (*e.g.*, by condensing in the manner shown in structure **IV**, Scheme 3), then cyclisation may be slower or a retro-Mannich reaction of the pendant propanal may occur to reform the methanimine. The formation of largely one isomer and its mirror image simply cannot be accidental, given the large number of theoretically possible products. As outlined above, the surprising regio- and stereo-selectivity can be rationalised in terms of a combination of thermodynamic and kinetically controlled condensation reactions governed by electronic, statistical and steric effects of the template and reagents.

Electrochemical reductions of the $[Pt(Me_5\text{-tricosatrieneN}_6)]^{4+}$ and $[Pt(Me_5\text{-tricosaneN}_6)]^{4+}$ complexes were irreversible $2e^-$ processes in aqueous media giving square planar Pt(II) complexes accompanied by dissociation of two nitrogen donor atoms. The trend to more positive reduction potentials for the Pt(IV) ions in the larger cage ligand relative to the smaller sar analogue is similar to that observed for Co(III), Rh(III) and Cr(III) cages as the cage cavity size was increased.[2,3,7,24] This is consistent with the larger cage's ability to more readily sustain a larger metal ion in its cavity.

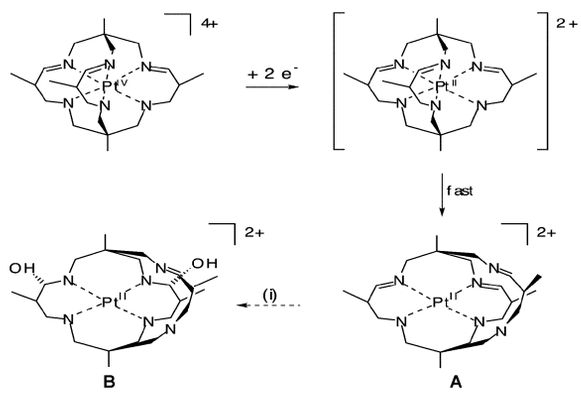

Scheme 5 Reduction of $[Pt^{IV}(Me_5\text{-tricosatrieneN}_6)]^{4+}$ (amine protons have been omitted for clarity). (i) Carbinolamine formation evident from hydrogenation of $[Pt^{IV}(Me_5\text{-tricosatrieneN}_6)]^{4+}$.

The reduction to Pt(II) imposes specific steric demands on the macrobicyclic ligand which results eventually in net dissociation of one strand of the ligand, *i.e.*, two *cis* nitrogen donor atoms are dissociated from the Pt(II) atom. A pathway for reduction to square planar Pt(II) is outlined in Scheme 5. This mechanism is argued to be similar to that for the dissociation proposed for the hydrogenation reaction which was monitored by NMR spectroscopy since similar Pt(IV) hexaamine cage complexes have shown that hydrogenation and bulk electrochemical reduction generate the same Pt(II) product.[2,25] The ^{13}C NMR spectra acquired during the hydrogenation of $[Pt(Me_5\text{-tricosatrieneN}_6)]^{4+}$ imply that the initial observed Pt(II) complex has a pseudo mirror-plane. This can only be accommodated if two nitrogen donor atoms *cis* to each other on the same strand dissociate to form species **A**. Dissociation of two nitrogen atoms *trans* to each other cannot produce the observed pseudo-symmetry directly since necessarily one nitrogen atom must be saturated and the other imine in character. Dissociation of one strand, however, does give a near-symmetrical product where the carbon atoms in the coordinated macrocycle on either side of the strand could be expected to have very similar NMR chemical shifts. Initially, however, it is most likely that two *trans* nitrogen donor atoms dissociate, followed by rapid re-addition of one of these donor atoms at Pt(II) and displacement of another nitrogen donor to give the product with pseudo-mirror symmetry. This should be a rapid process, given that the substituting nitrogen donor atom is tethered by the cage and poised for such an intramolecular attack at the Pt(II) ion but there is no direct evidence for such an intermediate. Moreover, the system is not amenable to detailed study since the observed product

was not stable enough to be isolated and reacted further to produce other complexes too numerous to unravel. The mechanistic proposal for the *trans* to *cis* rearrangement has precedent in the reduction of the $[Pt(en)_3]^{4+}$ ion.[20] In neutral conditions, $[Pt(en)_2]^{2+}$ and dissociated 1,2-ethanediamine are produced but in acidic conditions, the di-protonated bis-monodentate product $[Pt(en)(enH)_2]^{4+}$ has been isolated. In this instance, protonation of the pendant amines clearly slows the subsequent intramolecular amine addition to give the more stable square planar $[Pt(en)_2]^{2+}$ ion and free ligand.

The electrochemical reduction of $[Pt(Me_5\text{-tricosaneN}_6)]^{4+}$ was rather similar. At least, it showed an irreversible Pt(IV) reduction to the square planar Pt(II) species and there was no sign of an accessible Pt(III) intermediate. The failure to stabilize the elusive Pt(III) state in aqueous media at ambient temperature was disappointing. However, reduction of Pt(IV) did not lead immediately to rupture of the larger ligand framework in contrast to the sar analogues. In this respect at least one of our premises for this study was correct. Clearly, addition of the second electron is a very favoured process and also net dissociation of one strand of the cage to give the square planar Pt(II) complex is relatively facile.

Introduction of more polarisable donor atoms such as sulfur may help stabilise the Pt(III) in an octahedral environment and provide more reversible electrochemistry. Such molecules could be useful in electro- or photo-chemically driven systems for splitting water. Despite the disappointing electrochemical results, the study reflects the power of the template synthetic approach to rapidly generate stable macrobicyclic cage molecules in one process in relatively high yields and with remarkable specificity.

Experimental

Synthesis

All chemicals were AR grade unless otherwise specified. Bio-Rad analytical grade Dowex 50W-X2 (200–400 mesh, H^+ form) and SP-Sephadex C-25 (Na^+ form) ion-exchange resins were employed for the cation exchange chromatography. All condensation reactions were performed and quenched in the dark to limit any photoinduced decomposition. The synthesis of $[Pt(tame)_2]Cl_4{\cdot}H_2O$ has been described previously.[20]

(1,5,9,13,20-Pentamethyl-3,7,11,15,18,22-hexaazabicyclo-[7.7.7]tricosa-3,18,15-triene)platinum(IV) tetrachloride ($[Pt(Me_5\text{-tricosatrieneN}_6)]Cl_4{\cdot}5H_2O{\cdot}0.5HCl$). $[Pt(tame)_2]Cl_4{\cdot}H_2O$ (2 g) suspended in acetonitrile (20 mL) was added to a stirring suspension of anhydrous $NaClO_4$ (4 g) in acetonitrile (15 mL). After cooling in an ice bath, triethylamine (3 equivalents, 1.5 mL) was added dropwise. An orange colour developed, indicating that deprotonation had taken place, then aqueous formaldehyde (37%, 5 equivalents, 1.4 mL) followed by propanal (15 equivalents, 3.8 mL) were added. The reaction was stirred for three hours then quenched with concentrated HCl (~ 2 mL), resulting in a colourless suspension in a brown mother liquor. This reaction mixture was diluted to 1 L (water) and loaded onto a column of Dowex 50 W-X2 cation exchange resin (5 x 10 cm). After washing with water (1 L) and 1 M HCl (1 L), the complex was eluted with 6 M HCl. Evaporation of the eluate to near dryness yielded a white suspension, which was filtered and washed with a small amount of ethanol. The resulting powder was recrystallised from water and concentrated HCl, to yield fragile colourless crystals which crumbled as they dried. Yield 50%. The same synthesis was carried out using the triflate salt of the template to give a similar yield. Anal. Calc. for $[C_{22}H_{42}Cl_4N_6Pt]{\cdot}5H_2O{\cdot}0.5HCl$: C, 31.61; H, 6.33; N, 10.05; Cl, 19.09. Found: C, 31.84; H, 6.53; N, 9.80; Cl, 19.04%. The chloride salt was converted to the tetrachlorozincate salt by dissolving $[Pt(Me_5\text{-tricosatrieneN}_6)]Cl_4$ (100 mg) in a minimum volume of water (2 mL) and adding ~ 0.3 mL of a solution containing $ZnCl_2$ in 4 M HCl (~5 g/100 mL). Crystals suitable for an X-ray crystallographic analysis were obtained after ~ 36 hours. These were filtered by gravity on filter paper and allowed to dry in air.

NMR (δ (ppm), 1 M DCl) $[Pt(Me_5\text{-tricosatrieneN}_6)]Cl_4$ ^{1}H: 1.12 (s, 1H, cap CH_3, H_{10}), 1.22 (s, 1H, cap_{imine} CH_3, H_1), 1.40 (s, 3H, strap CH_3, H_6), 2.16 (d of t, 1H, cap CH_2, H_{7a}), 2.21 (d of t, 1H, strap CH_2, H_{8a}), 2.86 (d, 1H, cap CH_2, H_{7b}), 3.16 (d, 1H, cap CH_2, H_{8b}), 3.84 (d of t, 1H, cap CH_2, H_{3a}), 4.39 (d, 1H, cap CH_2, H_{3b}), 8.86 (t, 1H, imine, H_4).^{13}C: 16.0 (s, strap CH_3, C_6), 21.6 (s, cap CH_3, C_{10}), 22.2 (s, cap CH_3, C_1), 35.0 (broad t, strap CH/CD, C_5), 40.1 (t, quaternary, C_2), 42.2 (t, quaternary, C_9), 55.7 (s, strap CH_2, C_7), 56.3 (s, cap CH_2, C_8), 65.9 (t, cap CH_2, C_3), 189.5 (s, C_{imine}, C_4).

$^2J_{H-H}$ (Hz): $^2J_{3a-3b}$ = 14.1; $^2J_{7a-7b}$ = 16.2; $^2J_{8a-8b}$ = 14.4. $^3J_{Pt-H}$ (Hz): $^3J_{Pt-3a}$ = 42; $^3J_{Pt-4}$ = 69.2; $^3J_{Pt-7a}$ = 57.5; $^3J_{Pt-8a}$ = 54.4. $^4J_{H-H}$(Hz): $^4J_{3a-4}$ = 2.8; $^4J_{3b-4}$ = 4.9; $^4J_{4-7a}$ = 4.4. $^2J_{Pt-C}$ (Hz): $^2J_{Pt-C3}$ = 19.6. $^3J_{Pt-C}$ (Hz): $^3J_{Pt-C2}$ = 37.9; $^3J_{Pt-C5}$ = 25.1; $^3J_{Pt-C9}$ = 54.8.

Hydrogenation of $[Pt(Me_5\text{-tricosatrieneN}_6)]Cl_4$. The complex (50 mg) was dissolved in D_2O (0.5 mL) in an NMR tube and the Pd/C catalyst (10%, ~ 5 mg) was introduced. The suspension was purged gently with argon for 20 minutes. The NMR tube was sealed with Parafilm and then centrifuged for five minutes before the ^{1}H and ^{13}C NMR spectra were acquired. The sample was purged gently with dihydrogen for 30 minutes and again with argon for five minutes. After centrifugation, the ^{1}H and ^{13}C NMR spectra were acquired. The sample was then purged with dihydrogen for a further 1.5 h, then with argon (5 min) and the NMR spectra acquired after centrifugation. Finally, dihydrogen was bubbled gently through the sample for 16 hours, and the NMR spectra acquired after the usual argon and centrifuge treatment.

NMR (δ (ppm), D_2O) ^{1}H: After 2 hours H_2 purging, new signals appeared at 0.91 (s, CH_3), 0.98 (s, CH_3), 1.44 (s, CH_3), multiplet centred at 4.0, 4.98 (s, tentatively CHOH), 8.39 (s, imine). ^{13}C: 14.0, 14.6, 14.7, 17.8, 23.1, 38.5, 39.0, 44.7, 51.7, 56.4, 57.2, 68.4, 68.7, 94.6, 182.3.

(1,5,9,13,20-Pentamethyl-3,7,11,15,18,22-hexaazabicyclo-[7.7.7]tricosane)platinum(IV) tetrachloride ($[Pt(Me_5\text{-tricosaneN}_6)]Cl_4$). $[Pt(Me_5\text{-tricosatrieneN}_6)](ZnCl_4)_{1.5}{\cdot}Cl{\cdot}2H_2O$ (30 mg) was dissolved in a minimum volume of water and the pH of the solution was adjusted to 12.5 using Na_2CO_3. The solution was treated with $NaBH_4$ (2 mg) for 15 seconds and immediately sorbed onto Dowex (50W-X2) cation exchange resin (Na^+ form, 5 mL), with suction. The column was then washed thoroughly and quickly with water (500 mL) using the aspirator and then with 1 M HCl (200 mL) at atmospheric pressure. Elution with 6 M HCl and evaporation to dryness yielded a colourless powder of pure $[Pt(Me_5\text{-tricosaneN}_6)]Cl_4$, (yield 90%). A single light orange crystal of the Me_5-tricosane complex containing some of the deprotonated cation was slowly grown from a solution of $ZnCl_2$ in 4 M HCl (~ 5 g/100 mL). This was used for the crystallographic analysis.

NMR (δ (ppm), 1 M DCl) $[Pt(Me_5\text{-tricosaneN}_6)]Cl_4$ ^{1}H: 1.08 (d of d, 3H, strap CH_3, H_6, ^3J = 6.9 Hz, ^4J = 0.8 Hz), 1.16 (s, 1H, cap CH_3), 1.18 (s, 1H, cap CH_3), 2.36 (d of d, 1H, strap CH_2, ^2J = 14.2 Hz, $^3J_{Pt-H}$ = 31.5 Hz), 2.45–2.60 (unresolved multiplet, 2H, overlapping strap CH (H_5) and strap CH_2), 2.69 (d of d, 1H, cap CH_2, ^2J = 14.5 Hz, $^3J_{Pt-H}$ = 39.2 Hz), 2.78–2.92 (multiplet, 2H, overlapping strap CH_2 and cap CH_2), 3.36 (d, 1H, cap CH_2, ^2J = 14.5 Hz), 3.41 (d of d, 1H, strap CH_2, ^2J = 14.5 Hz), 3.69 (d, 1H, cap CH_2, ^2J = 14.2 Hz).

^{13}C: 16.8 (s, strap CH_3, C_6), 21.7 (broad s, cap CH_3, C_1 and C_{10}), 29.4 (t, CH, C_5, $^3J_{Pt-C}$ = 21 Hz), 38.6 (t, quaternary, C_2 or C_9, $^3J_{Pt-C}$ = 41 Hz), 45.5 (t, quaternary, C_2 or C_9, $^3J_{Pt-C}$ = 86 Hz), 56.9 (t, cap CH_2, $^2J_{Pt-C}$ = 13 Hz), 57.7 (t, strap

CH_2, $^2J_{Pt-C}$ = 10 Hz), 58.1 (t, cap CH_2, $^2J_{Pt-C}$ = 15 Hz), 64.8 (t, strap CH_2, $^2J_{Pt-C}$ = 11 Hz).

Physical methods

All ^1H and ^{13}C NMR spectra were acquired using Varian Gemini 300 MHz, Varian VXR 300 MHz or Varian VXRS 500 MHz spectrometers and standard Varian software. D_2O and DCl (Merck) were used without further purification. All spectra were referenced internally against 1,4-dioxane (3.744 ppm *vs.* $(CH_3)_4Si$ for the ^1H NMR spectra and 67.4 ppm *vs.* $(CH_3)_4Si$ for ^{13}C NMR spectra). The two-dimensional experiments were obtained with Varian VXR 300 MHz or Varian VXR 500 MHz spectrometers in conjunction with standard Varian software. The pre-transient delay times ($d1$) and recycling times for the experiments were typically 0.5–2 s and 1–6 s, respectively. Sinebell weighting functions were used in both dimensions prior to Fourier transformation for DQF COSY, HMQC and HMBC spectra. Milli-Q water was used for the aqueous electrochemistry, and the acetone was distilled over P_2O_5. The electrolytes used in the aqueous electrochemistry were AR grade. The electrolyte concentration was either 0.1 or 1.0 M. The concentration of the electroactive species was ~ 0.3 mM. The samples were purged for ~ 15 minutes with a continuous flow of argon or dinitrogen prior to data acquisition. Measurements were acquired under a blanket of dinitrogen or argon at 293 ± 1 K unless otherwise specified. Since the reference electrodes varied, in order to allow comparison between experiments, the potentials cited in the text are referenced to the standard hydrogen electrode (SHE) unless otherwise specified.

The cyclic voltammograms using a mercury drop working electrode were recorded using a Princeton Applied Research Model-170 Polarographic Analyser or Model-173 Universal Programmer in conjunction with a Model-175 Potentiostat/Galvanostat. Both systems were interfaced with a Hewlett-Packard 7046A (X,Y) plotter. The mercury electrode (Metrohm 663 VA stand, interfaced with a Research School of Chemistry interface unit Model-411) was used in the HMDE mode. The three-electrode configuration included an auxiliary electrode, which was a carbon rod (~ 0.4 cm diameter, ~ 8 cm in length), and the reference electrode, which was either a Ag/AgCl/KCl(sat) (199 mV *vs.* SHE) or a saturated calomel electrode (SCE, 241 mV *vs.* SHE).[26] The reference electrodes were separated from the cell using a salt bridge containing an aqueous solution of 1.5 M NaCl.

The electrochemical measurements using disc electrodes were recorded with a BAS-100 Electrochemical Analyser. The three-electrode configuration comprised a platinum wire auxiliary electrode (0.5 mm diameter, ~ 4 cm in length) and a working electrode, which was either a BAS glassy carbon, a platinum, edge-plane pyrolytic graphite (EPG) or a gold (1.5 mm) disc electrode. These were polished using an aqueous suspension of BAS polishing alumina on a clean polishing cloth. The electrode was then rinsed thoroughly with distilled water and carefully wiped dry with lens tissue. The reference electrodes were either a Ag/AgCl/KCl(sat) or a SCE and were separated from the cell using a salt bridge containing an aqueous solution of 1.5 M NaCl. In acetone, the reference electrode was a Ag/AgCl/LiCl(sat. acetone) electrode.

Structure determination¶

The structure of $[Pt(Me_5\text{-tricosatrieneN}_6)](ZnCl)_{1.5}Cl\cdot 2H_2O$ was determined using an Enraf-Nonius CAD-4 four circle diffractometer and graphite monochromated MoK_α radiation. The platinum atom position was readily determined and the positions of the non hydrogen cation atoms were obtained from standard electron density maps. The platinum site causes data with $l = 4n$ to be much stronger than the remaining data. The interpretation of the remaining atom sites required sensible chemical reasoning to initiate parameters for the subsequent least squares refinement using the constrained least squares refinement program *RAELS92*.[27] A necessary first step was the recognition of the $ZnCl_4^{2-}$ anion disordered about a two-fold axis. The Zn(1) and Cl(3) atoms were well resolved but the Cl(1) atom lay very close to the axis and atoms Cl(2) and Cl(4) were approximately two-fold related. Restraints were used to control the coordinates of atoms Cl(1), Cl(2) and Cl(4), making differences in Zn–Cl bond distances approach zero. Weak restraints on differences between Cl–Zn–Cl bond angles were also used. Quoted errors on these distances and angles assume an appropriateness for these restraints. A 15-parameter rigid body TLX constraint was used for the thermal motion of the $ZnCl_4^{2-}$ anion.[27] Anisotropic thermal parameters were used for all atoms. The thermal motion of the atom O(2) was constrained to have the same symmetry as that implied by the two-fold symmetry site about which it was disordered. The atom O(1) was constrained to have the same thermal motion as the Cl(5) atom on approximately the same site. Hydrogen atoms were given the same thermal parameters as the atoms to which they were attached. They were included in chemically sensible positions which were recalculated each refinement cycle. A final value for $R_1 = \Sigma |\Delta F|/\Sigma |F_{obs}| = 0.046$ was obtained for the 1480 [$I > 3\sigma(I)$] independent reflections out of 2066 unique data.

The X-ray crystallographic data for the $[Pt(Me_5\text{-tricosane-}N_6)]$ complex were collected using a Rigaku AFC6S diffractometer and the conditions described in Table 2. The intensities of three representative reflections were measured after every 150 reflections. Over the course of data collection, the standards decreased by 1.7% and a linear correction factor was applied to the data to account for this variation.

The crystal structure contains three counter ions per Pt(IV) complex. These counter ions take up positions consistent with maintaining the inherent three-fold rotation symmetry of the complex creating 6 N–H ··· Cl hydrogen bonds, two per anion, *viz*. Cl(11), Cl(12), Cl(21), Cl(22), Cl(31), Cl(32). In the absence of deprotonation at any of the ligand N atoms, the Pt(IV) complex cation has a formal charge of +4, requiring one $[ZnCl_4]^{2-}$ ion and two $[ZnCl_3(H_2O)]^-$ ions. If one N atom is deprotonated per ligand, the cation has a formal charge of 3+ requiring three $[ZnCl_3(H_2O)]^-$ ions. The crystal was refined as a 0.88(1) : 0.12 mixture of these two options. The dianion Zn(1), Cl(11), Cl(12), Cl(13), Cl(14) was partially replaced by a mono-anion with atom sites Zn(1′), Cl(11), Cl(12), Cl(13′), O(1′) where the Cl(11) and Cl(12) were regarded as common to both species. Note that all 6 NH have Cl atoms in hydrogen bonding positions and all the N sites are essentially tetrahedral.

On deprotonation of the cation, the $[ZnCl_4]^{2-}$ counter ion is replaced by $[ZnCl_3(H_2O)]^-$ and it is reasonable to expect the Zn to be displaced somewhat. Using just $[ZnCl_4]^{2-}$ for the first counter ion, refinement reached $R = 0.035$ but gave a difference map with a large peak of 2.8 e Å^{-3} (compared with −0.8 for minimum on final map) 1.27 Å away from Zn(1). This peak and Zn(1) were at essentially the same distance from the Pt. Assuming the peak to be Zn(1′), it was possible to locate a $[ZnCl_3(H_2O)]^-$ ion using two minor peaks on the difference map (with appropriate peak height ratios) together with the already existing Cl(11) and Cl(12) sites. This model refined to $R = 0.027$ with an occupancy ratio of 0.88(1) : 0.12 for $[ZnCl_4]^{2-}$: $[ZnCl_3(H_2O)]^-$. The angles around Zn(4) were reasonable but the Zn(1′)–Cl(11) and Zn(1′)–Cl(12) distances were 2.49(1) and 2.16(1) Å respectively, implying that the minor occupancy components at these Cl sites could be moved along the bond directions by up to 0.2 Å, with some associated adjustment of the minor cation component.

¶ CCDC reference numbers 202905 and 205497. See http://www.rsc.org/suppdata/ob/b2/b212326f/ for crystallographic files in .cif or other electronic format.

Refining the cation as two species was not feasible. Refinement assuming just a single species, located atoms at positions of maximal probability. Thus only the major component was well defined. No further refinement was attempted since the extended model and the improved *R* factor provided a good fit to the data as well as a satisfactory explanation for the orange colouration arising from some deprotonation of the cation.

The data were corrected for Lorentz and polarisation effects. The structure was solved by direct methods[28] and expanded using Fourier techniques.[29] The non-hydrogen atoms were refined anisotropically. Hydrogen atoms were included but not refined. Neutral atom scattering factors were taken from Cromer and Waber.[30] Anomalous dispersion effects were included in *F*calc[31] and the values for $\Delta f'$ and $\Delta f''$ were those of Creagh and McAuley.[32] The values for the mass attenuation coefficients were those of Creagh and Hubbel.[33]

Acknowledgements

Support and help from the Australian Research Council, Professor Alan Bond, Monash University, Dr Chunnian Shi and Professor Fred Anson, California Institute of Technology, the ANU Microanalytical Service and the ANU NMR centre are gratefully acknowledged.

References

1 K. N. Brown, R. J. Geue, T. W. Hambley, A. M. Sargeson and A. C. Willis, *Chem. Commun.*, 1996, 567.
2 K. N. Brown, PhD Thesis, Australian National University, 1994.
3 R. J. Geue, A. Höhn, S. F. Ralph, A. M. Sargeson and A. C. Willis, *J. Chem. Soc., Chem. Commun.*, 1994, 1513.
4 I. I. Creaser, R. J. Geue, J. M. Harrowfield, A. J. Herlt, A. M. Sargeson, M. R. Snow and J. Springborg, *J. Am. Chem. Soc.*, 1982, **104**, 6016.
5 A. M. Bond, G. A. Lawrance, P. A. Lay and A. M. Sargeson, *Inorg. Chem.*, 1983, **22**, 2010.
6 J. M. Harrowfield, A. J. Herlt, P. A. Lay, A. M. Sargeson, A. M. Bond, W. A. Mulac and J. C. Sullivan, *J. Am. Chem. Soc.*, 1983, **105**, 5503.
7 R. J. Geue, M. B. McDonnell, A. W. H. Mau, A. M. Sargeson and A. C. Willis, *J. Chem. Soc., Chem. Commun.*, 1994, 667 and references therein.
8 P. A. Lay, PhD Thesis, Australian National University, 1981, Chapter 5.
9 H. A. Boucher, G. A. Lawrance, P. A. Lay, A. M. Sargeson, A. M. Bond, J. C. Sangster and J. C. Sullivan, *J. Am. Chem. Soc.*, 1983, **105**, 4562.
10 K. S. Hagen, P. A. Lay and A. M. Sargeson, *Inorg. Chem.*, 1988, **27**, 3423.
11 K. K. Pandey, *Coord. Chem. Rev.*, 1992, **121**, 1 and references therein.
12 D. Pearce, PhD Thesis, Research School of Chemistry, Australian National University, 1996, and references therein.
13 K. Drok, J. M. Harrowfield, S. J. McNiven, A. M. Sargeson, B. W. Skelton and A. H. White, *Aust. J. Chem.*, 1993, **46**, 1557 and references therein.
14 J. M. Harrowfield and A. M. Sargeson, *J. Am. Chem. Soc.*, 1974, **96**, 2634.
15 A. Höhn, R. J. Geue and A. M. Sargeson, *J. Chem. Soc., Chem. Commun.*, 1990, 1473.
16 J.-M. Le Parco, L. McIntyre and R. Freeman, *J. Magn. Reson.*, 1992, **97**, 553 and references therein.
17 H. Günter, *NMR Spectroscopy, An Introduction*, John Wiley and Sons, New York, 1973, 2nd edn., chapter 4.
18 P. A. Lay and A. M. Sargeson, *Inorg. Chem.*, 1986, **25**, 4801.
19 No responses were observed using glassy carbon or platinum disc electrodes in the cyclic voltammograms (CV's) of [Pt(Me_5-tricosatrieneN$_6$)]Cl_4 in 0.1 M NaCl, 0.1 M $NaClO_4$, 0.1 M HCl and 0.1 M $HClO_4$ from 0 to ± 1.0 V (*vs.* SCE).
20 K. N. Brown, D. C. R. Hockless and A. M. Sargeson, *J. Chem. Soc., Dalton Trans.*, 1999, 2171.
21 K. N. Brown, D. R. Hockless, A. M. Sargeson, manuscript in preparation.
22 O. N. Adrianova and T. N. Fedotova, *Russ. J. Inorg. Chem.*, 1970, **15**, 1272.
23 O. N. Adrianova and T. N. Fedotova, *Russ. J. Inorg. Chem.*, 1980, **25**, 105.
24 K. N. Brown, D. C. R. Hockless, S. F. Ralph, H. Riesen, A. M. Sargeson, manuscript in preparation.
25 Although the reduction of [Pt(tetracosanediimineN$_6$)]$^{4+}$ cage complexes to Pt(II) is accompanied by *trans* dissociation of the nitrogen donors, the same product was isolated from both the hydrogenation and the bulk electrochemical reduction of the parent Pt(IV) complex.
26 D. R. Lide, *CRC Handbook of Chemistry and Physics*, 73rd edn., CRC Publishing Co., Boca Raton, 1992–1993, and references therein.
27 A. D. Rae, RAELS 92, A Comprehensive Constrained Least Squares Refinement Program, Australian National University, 1992.
28 A. Altomare, M. Cascarano, C. Giacovazzo and A. Guagliardi, *J. Appl. Crystallogr.*, 1993, **26**, 343.
29 P. T. Beurskens, G. Admiraal, G. Beurskens, W. P. Bosman, R. de Gelder, R. Israel, J. M. M. Smits, *DIRIF94: The DIRDIF-94 program system, Technical Report of the Crystallography Laboratory*, University of Nijmegen, The Netherlands, 1994.
30 D. T. Cromer, J. T. Waber, *International Tables for X-ray Crystallography*, Kynoch Press, Birmingham, 1974, vol. 4, Table 2.2 A.
31 J. A. Ibers and W. C. Hamilton, *Acta Crystallogr.*, 1964, **17**, 781.
32 D. C. Creagh, W. J. McAuley, *International Tables for Crystallography*, Kluwer Academic Publishers, Boston, 1992, Vol. C, Table 4.2.6.8, pp. 219–222.
33 D. C. Creagh, J. H. Hubbel, *International Tables for Crystallography*, Kluwer Academic Publishers, Boston, 1992, Vol. C, Table 4.2.4.3, pp. 200–206.